Astron. Astrophys. 343, L40–L44 (1999)

ASTRONOMY AND ASTROPHYSICS

LETTER

Letter to the Editor

Lyα emission at $z \sim z_{\rm em}$ around the quasar J2233−606 in the Hubble Deep Field South⋆

J. Bergeron[1], **P. Petitjean**[2,3], **S. Cristiani**[1,4], **S. Arnouts**[4], **F. Bresolin**[1], **and G. Fasano**[5]

[1] European Southern Observatory, Karl-Schwarzschild-Strasse 2, D-85748 Garching, Germany
[2] Institut d'Astrophysique de Paris, CNRS, 98 bis Boulevard Arago, F-75014 Paris, France
[3] UA CNRS 173- DAEC, Observatoire de Paris-Meudon, F-92195 Meudon Cedex, France
[4] Università di Padova, Vicolo dell'Osservatorio 5, I-35122 Padova, Italy
[5] Osservatorio Astronomico, Vicolo dell'Osservatorio 5, I-35122 Padova, Italy

Received 4 December 1998 / Accepted 8 January 1999

Abstract. The STIS Hubble Deep Field South around the quasar J2233−606 was observed in the course of the VLT-UT1 Science Verification programme with the Test Camera in two broad-band filters, B and R, and in a narrow-band filter roughly centered at the quasar emission redshift, $z_{\rm em} = 2.238$. The most striking result is the discovery of a giant Lyα nebulosity around this radio-weak quasar, with an overall extent of $9.2'' \times 12.1''$ or 121×159 h_{50}^{-2} kpc^2 and a luminosity of 3.1 $\times 10^{44}$ h_{50}^{-2} erg s^{-1} (for q_0 = 0), similar to those found around radio-loud quasars and radio galaxies. There are three additional emission-line candidates in a $1.11' \times 1.24'$ field with an observed Lyα flux above our 3σ Lyα detection limit of 1.9×10^{-17} erg s^{-1} cm^{-2} for point sources. The resolved bright object located 4.9″ north-east of the quasar, which has recently been identified as a galaxy at $z_{\rm g}$ = 0.57, has an associated, weak Mg II absorption in the quasar spectrum.

Key words: cosmology: observations – galaxies: quasars: general – galaxies: halos – galaxies: clusters: general

1. Introduction

Several techniques have been used to study the history of galaxy formation from the Lyman-break galaxies (Steidel et al. 1996a, 1996b, 1998) to the Lyα emitters (Hu et al. 1998) in different environments. The global star formation history inferred from the Lyman-break galaxy sample and other surveys at lower redshift shows a peak at $z \sim$ 1-2 followed by a flattening or possibly a plateau at higher redshifts (Madau et al. 1996, 1998). Predictions derived from hierarchical models of galaxy formation (Baugh et al. 1998; Mo et al. 1998) are broadly in agreement with this result. The quasar comoving density appears also to be correlated to the global star formation history (Madau et al. 1998).

At high redshift, rich environments appear to be traced by quasars and radio galaxies (Hu et al. 1991; Heckman et al. 1991a, 1991b; Hu & McMahon 1996; McCarthy et al. 1995, 1996). Discoveries of close companion galaxies and extended nebulosities around high-redshift quasars support the assumption of strong tidal interaction between the quasars and their companions, thus the formation models with merging of subgalactic clumps (e.g. Petitjean et al. 1996, Omont et al. 1996).

Spectacular emission-line nebulosities associated with radio galaxies have been discovered since the mid-1980s (see McCarthy et al. 1995 and references therein). Searches for "fuzz" and companion galaxies around high-redshift quasars have been conducted mainly for radio-loud quasars to test the assumption that radio-loud quasars and radio galaxies are the same class of objects viewed along various lines of sight with respect to the radio axis. A few Lyα nebulosities and/or companion galaxies have been detected in samples of radio-quiet quasars (Hu et al. 1991, Bremer et al. 1992, Petitjean et al. 1996), but they are not as common as those found around radio-loud quasars.

The goal of this project is to investigate the close environment of the quasar in the Hubble Deep Field - South (HDF-S). The synergy between the HST and ground-based telescopes has produced breakthrough results in galaxy formation and the presence of a quasar in the HDF-S opens further possibilities to investigate the properties of young galaxies and Lyα emitters.

The HDF-S quasar, J2233−606, is radio weak with a detected flux of 1.0 mJy at 1.4 GHz (Hopkins 1998) and would thus fall in the category previously defined as radio-quiet. The quasar field was observed during the VLT-UT1 Science Verification programme with the Test Camera in two broad-band filters, B and R, and in a narrow-band filter roughly centered at the quasar emission redshift, $z_{\rm em} = 2.238$ (Sealey et al. 1998). The observations and data analysis are described in Sect. 2, their implications are given in Sect. 3 and the conclusions are presented in Sect. 4.

Send offprint requests to: J. Bergeron

⋆ Based on observations collected at the European Southern Observatory, Paranal, Chile.

2. Observations and data analysis

The observations were carried out with the VLT-UT1, as part of the Science Verification programme on 30 August and 1 September 1998. The Test Camera CCD, $(2k)^2$, was binned 2×2 which gives a pixel scale of 0.091″ and a 1.54′ square field of view. The exposures were of 17×881.8 sec for the narrow-band filter (NB: $\lambda_{\rm c} = 3913$Å, $\Delta\lambda = 86$Å), 3×600 sec and 8×900 sec for the Bessell B and R filters respectively. A shifting pattern was performed between all the individual images. Observations of several standard stars were carried out for each filter, including two spectrophotometric standard stars for the NB filter. All data calibration was done by the Science Verification team and the final products were released to the community on 2 October 1998.

The response of the Test Camera CCD is inhomogeneous with patches of lower sensitivity. The flat-fielding procedure led to well corrected B and R images but some large-scale residual variations remain in the NB images. The point spread function (PSF) also shows some small gradient across the field. The combined field for the NB images is $1.11' \times 1.24'$. The resolution for the combined frames is 0.65″, 0.70″ and 0.90″ for the NB, B and R filters respectively. The PSF is close to circular for the NB and R filters, but varies from circular to squarish with increasing radius for the B filter.

Two methods were applied to search for the Lyα emitters. First, the B image was subtracted from the NB image after applying a scaling factor, derived from the calibration of the spectrophotometric standard stars, and resampling to co-align the two images. Secondly, the B and R magnitudes derived from the Sextractor software (Bertin & Arnouts 1996) analysis were used for continuum subtraction from the NB magnitudes. While the latter method has the advantage of accounting for colour-term corrections, the former, although leading to a slight increase in the overall noise, has the advantage of taking into account possible differences in the spatial gradients of the continuum and line emission of resolved objects. For a 2 FWHM aperture, the 3σ detection magnitude limits are 27.3 and 26.6 for the B and R images respectively. The 3σ detection flux limit, as derived from the Lyα continuum-free image is 1.9×10^{-17} erg cm^{-2} s^{-1} for a point source, and the surface brightness 3σ limit is 4.5×10^{-17} erg cm^{-2} s^{-1} arcsec^{-2}.

The redshift range covered by the NB image is 2.183-2.254. It should be noted that the quasar emission redshift is uncertain. The mean redshift derived from the high ionization lines C IV, C III] + Al III ($z_{\rm em}$ = 2.237) is smaller than that derived from Mg II ($z_{\rm em}$ = 2.252) by about 1390 km s^{-1} (Sealey et al. 1998). This is consistent with the usual observation that high-ionization lines are blueshifted compared to low-ionization ones (Espey et al. 1989). Infrared spectroscopy of quasars has shown that the redshifts of forbidden lines are similar to those of low-ionization lines (Carswell et al. 1991). This suggests that the Lyα emission associated with the quasar should be centered at about 3951 Å, a wavelength which is very close to the peak of the quasar spectrum observed by Outram et al. (1998). Therefore, it cannot be excluded that only part of the Lyα emission by gas surrounding the quasar and nearby galaxies can be detected by our observations.

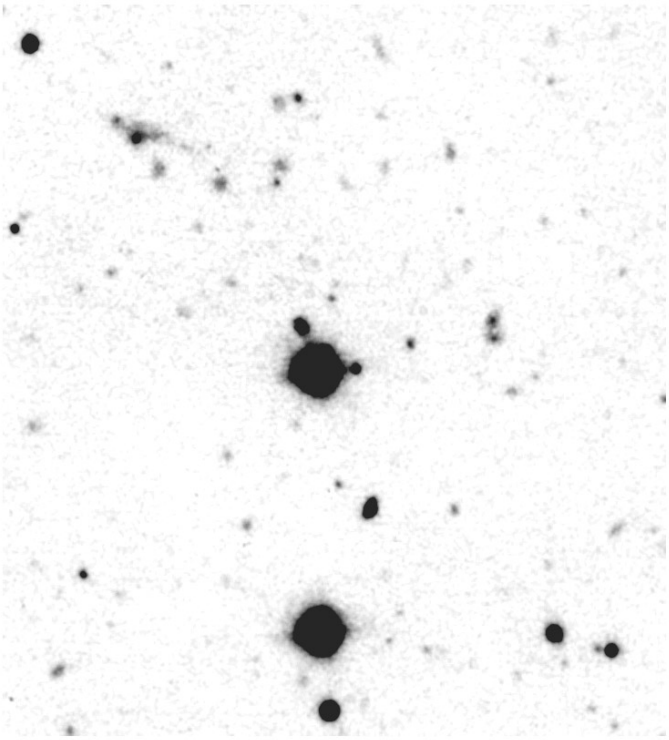

Fig. 1. B-band image of a $66.3'' \times 73.1''$ field around the quasar J2233−606 in the HDF-S. North is to the top and east to the left.

3. The Lyα emitters

The B image is shown in Fig. 1 and the result of the continuum subtraction from the NB image is shown in Fig. 2. A Gaussian smoothing has been applied to the latter with a σ=1.5 pixel, and the signal above 1σ only is displayed. A large patch of lower sensitivity, which could not be corrected by the flat-fielding procedure, is seen to the east of the quasar. Three stars (one north-east and two south-west) have very blue colours and clearly show a positive signal in the NB−B image. There is also some residual emission from the star 3.8″ west to the quasar. The other stars have much redder colours, including the brigthest one in the B image, and show a negative signal in the NB−B image.

The most striking feature is the discovery of a giant Lyα nebulosity around the radio-weak quasar J2233−606, without associated continuum emission in the B or R bands. The overall extent of this nebulosity down to the 3σ surface brightness detection limit is $9.2'' \times 12.1''$ or 121×159 h_{50}^{-2} kpc^2 for q_0 = 0 (where h_{50} is the Hubble constant in units of 50 km s^{-1} Mpc^{-1}). The central unresolved excess includes flux from both the quasar and the inner part of the Lyα nebulosity/galaxy host. It should be noted that no significant narrow Lyα emission is present in the quasar spectrum, since the observed complex Lyα profile (Sealey et al. 1998; Savaglio 1998) can be fully accounted for by the several strong absorption lines detected close to the peak of the broad Lyα component by Outram et al. (1998).

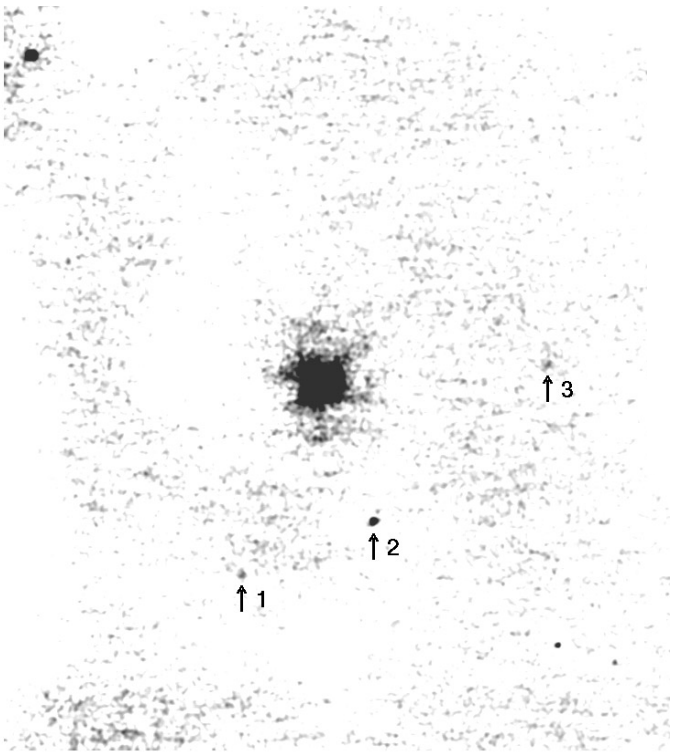

Fig. 2. NB−B image of a $66.3'' \times 74.5''$ field around the quasar J2233−606. The three galaxies detected in this image, in addition to the quasar fuzz, are labelled. The other detected objects are stars with very blue colours (see text). North is to the top and east to the left.

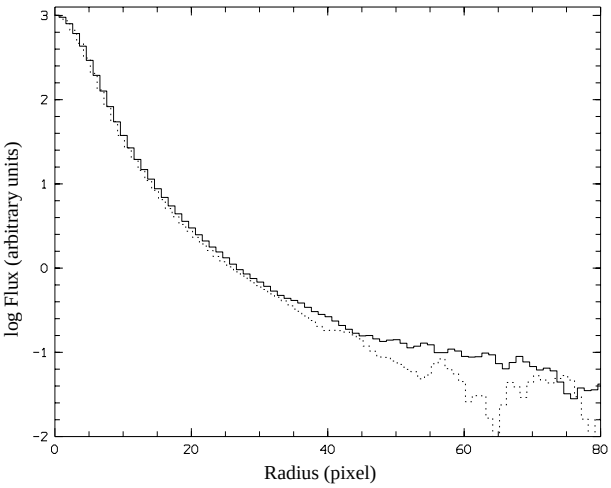

Fig. 3. B-band isophotal profiles of the quasar (thick line) and the brigthest southern star (dashed line).

To confirm the existence of the giant Lyα nebulosity and derive the radius at which the Lyα flux from the giant nebulosity exceeds that from the unresolved component, we have compared the isophotal profile of the quasar with that of a bright star. This method has not been applied to the R image, as the PSF is significantly broader (FWHM=0.90″) and the saturated, brightest southern star is blended with another star at the south edge of the field.

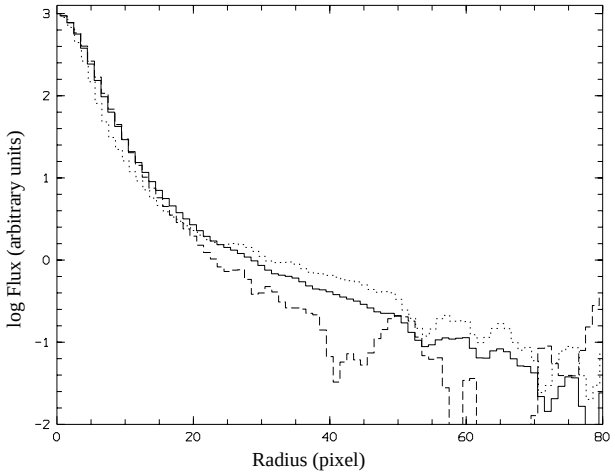

Fig. 4. Isophotal profiles of the quasar (thick line) and the brigthest southern star (dashed line) for the NB image and of the quasar for the NB−B image (dotted line).

The isophotal profiles of the quasar in the B, NB and NB−B image have been constructed avoiding regions where it could be contaminated by the closest galaxy at $4.9''$ to the north-east and the star at $3.8''$ to the west. The B-band isophotal profiles of the quasar and the brightest southern star are shown in Fig. 3. The two profiles have the same FWHM and no significant excess is detected at radial distances $r < 55$ px (or 5.00″). Beyond this radius the high noise level, especially around the bright star, prevents a meaningful comparison. Similar isophotal profiles are presented in Fig. 4 for the NB image together with that of the quasar for the NB−B image. A significant excess is seen in both the NB and NB−B quasar profiles beyond a radius of 25 px (or 2.28″). Beyond a radius of 50 px, the S/N ratio in the star profile is quite low and the background level poorly determined. It should be noted that the smaller FWHM of the quasar in the NB−B image as compared to the B image arises from the subtraction (photometric) of images with different spatial resolution and PSF shape.

The Lyα flux of the giant nebulosity beyond a radius of 2.28″ is given in Table 1. The Lyα luminosity equals (3.1 and 1.1) $\times 10^{44}\,{\rm h}_{50}^{-2}$ erg s^{-1} for $q_0 = 0$ and 0.5 respectively. Although very bright, extended Lyα envelopes have rarely been detected among the radio-quiet quasar population, the extent and Lyα luminosity of the gaseous envelope around the radio-weak quasar in the HDF-S are similar to those of the brighter nebulosities discovered around radio-loud quasars and radio galaxies (see e.g. Heckman et al. 1991b; McCarthy et al. 1995, 1996; van Ojik 1995; van Ojik et al. 1996). There is no detection of an underlying stellar component associated with this gaseous envelope. Its morphology is highly disturbed with external detached patches. The most striking ones are a structure elongated east-west located south of the quasar at a radial distance of 5.3″ and an emission clump just west of the bright galaxy located at a radial distance of 4.9″ north-east of the quasar. The B and R magnitudes of this galaxy are 23.03 and 21.84 respectively and its continuum emission extends over $\simeq 2.0''$. If the galaxy is at the

Table 1. Lyα emitters in the STIS field of the HDF-S

Object	$\Delta\alpha$ arcsec	$\Delta\delta$ arcsec	m(B) $\pm1\sigma$ rms	m(R) $\pm1\sigma$ rms	F(Lyα) 10^{-17} erg cm^{-2} s^{-1}
Quasar fuzz	$\geq$4.50	$\geq$4.50			320.0
Galaxy 1	7.89	−18.94	>27.3	>26.6	2.2
Galaxy 2	−5.21	−13.62	22.64±0.05	22.21±0.05	10.6
Galaxy 3	−22.40	+2.01	27.10±0.35	26.10±0.18	3.2

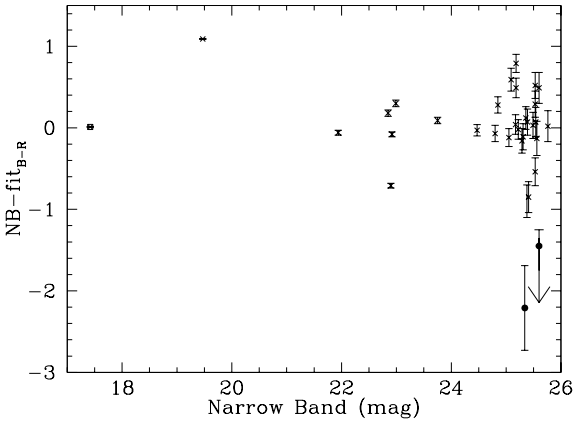

Fig. 5. Difference between observed NB magnitudes and expected magnitudes for objects with a continuous SED. Two candidate emission-line objects are shown as filled circles. The quasar is the brightest object in the left part of the diagram.

quasar redshift, its size and R-band absolute magnitude are 26 kpc and M(R)=−25.4 (for h_{50} = 1 and q_0 = 0). Consequently, we do not favor the possibility that gas is stripped out by tidal interaction between the quasar and this north-east object. The galaxy morphology is that of a barred spiral (as observed in the STIS very deep image of the HDF-S available at STScI since 23.09.1998) and, if at $z \sim 0.5$, its luminosity would be about that of a L* galaxy. The latter alternative has recently been confirmed and the measured redshift is equal to 0.57 (Tresse et al. 1998).

The Lyα emitter candidates detected in the NB−B image can be seen in Fig. 2. Their position relative to the quasar, B and R magnitudes as well as Lyα fluxes are given in Table 1. There are three detections above our 3σ Lyα flux limit of 1.9×10^{-17} erg s^{-1} cm^{-2} for point sources. As clearly seen in the STIS very deep image of the HDF-S, Galaxy 2 is resolved into three components, the northern one being detached from the main body of the galaxy. Its Lyα emission is only detected within the central brightest part of the galaxy. Galaxy 3 is marginally detected in the B and R images at about a 2σ level. Its presence is confirmed by the HDF-S/STIS image where it appears as a faint, very compact object. Galaxy 1 is detected at the 3.5σ level the in NB−B image, but it has no counterpart either in our B and R images or in the HDF-S/STIS image. To check whether the non-detection in the latter is consistent with the observed Lyα flux, we have used the STIS exposure time calculator. The result is that, if the object has a negligible continuum emission and is unresolved, it would have a S/N of 3, which is consistent with the uncertainty on our measured Lyα flux and the possibility that the line emission is extended as may be the case for Galaxy 3.

A search has also been carried out for emission-line candidates among all the objects detected in the NB frame above the 5σ confidence level (for a 2 FWHM aperture), that is with a NB flux above 2.5×10^{-17} erg s^{-1} cm^{-2}. For each object, we have estimated the expected continuum flux on the basis of a correlation between the B and R magnitudes and the corresponding NB magnitude. This relation was empirically calibrated by fitting the median NB−B as a function of B−R for the objects observed in the quasar field and is expected to correspond to a spectral energy distribution (SED) without emission features. For Galaxy 1, undetected in B and R, a B−R ≥ 0.0 lower limit has been assumed. Fig. 5 shows the difference between the observed and estimated NB magnitudes as a function of the NB magnitude. Two objects with a NB excess > 0.9 mag, roughly corresponding to a Lyα rest equivalent width of 50Å (see e.g. Hu et al. 1998), have been selected as candidate emission-line galaxies. They are Galaxies 1 and 3 of Table 1, already identified as candidate Lyα emitters in the analysis of the NB−B image. Galaxy 2 has not been selected since the source was not de-blended into subcomponents with the Sextractor algorithm and the total magnitudes of this complex object do not show a NB excess satisfying the above described selection criterion.

The difference between the integrated flux in the NB filter and the equivalent flux in the B filter (rescaled by the different equivalent passband of the filter) have also been computed from the Sextractor magnitudes. The zero points of the two flux-scales have been calibrated on the basis of the SED of the quasar and the response curves of the filters. The resulting Lyα fluxes agree to within roughly 15% with those estimated from the NB−B image subtraction.

4. Discussion

While searching for emission-line galaxies at the redshift, $z_{\rm em}$ = 2.238, of the radio-weak quasar J2233−606, we have discovered a spectacular Lyα nebulosity associated with this quasar. The very large extent, 121×159 h_{50}^{-2} kpc^2 (for q_0 = 0), and high Lyα luminosity, 3.1×10^{44} h_{50}^{-2} erg s^{-1} (beyond a radius of 2.28″) of this giant emission-line halo are much larger than usually found around objects of this class but similar to those for Lyα nebulae associated with radio-loud quasars and radio-galaxies (Heckman et al. 1991b; McCarthy et al. 1995). The morphology of

the latter is usually asymmetric and/or elongated along an axis that is roughly aligned with that of the radio source. In contrast, the outer parts of the halo around J2233−606 are patchy but on the whole fairly circular. Other properties may also differ, such as e.g. the gas velocity field. The extended emission-line gas associated with radio-loud objects often has spatially resolved velocities of 1000 km s^{-1} or more and in some cases there are detached Lyα regions with velocity differences of several 100 km s^{-1}. Spectroscopic follow-up of the gaseous nebulosity around J2233−606 will reveal whether its velocity dispersion and possibly its velocity field, observable in conditions of excellent seeing, are similar to those found for radio-loud objects or else of much smaller amplitude, i.e. whether it traces as a massive object as those inferred for the radio-loud population.

Three additional emission candidates have been detected within a field of 1.4 arcmin^2 down to a 3σ magnitude limit of 1.9×10^{-17} erg cm^{-2} s^{-1} for a point source of FWHM = 0.65″ (the outer parts of the combined NB image have a higher noise level). Galaxy 2 is brighter (B = 22.6) whereas Galaxies 1 and 3 are fainter than the high-redshift candidates selected by Lowenthal et al. (1997) in the HDF-N, all of which are in the magnitude range $24 < \mathrm{B} < 26$. These authors have found three of these candidates to be at redshifts $z \sim 2.25$, of which two have strong Lyα emission. It is apparent that Galaxy 2 is intriguingly bright (M(R) = −25.0 if at $z_{\rm g} = z_{\rm em}$). It is possible that an intervening object could be projected on top of the Lyα emitter. Indeed, the deep STIS image of the HDF-S shows that a complex object is present at the position of the emitter candidate that resembles a chain of objects. Alternatively, the detected emission line could be C III]λ1909, in which case the galaxy would be at $z_{\rm g}$ = 1.05 with an absolute magnitude M(R) = −22.6. Galaxy 3 is also seen in the deep STIS image and it is a faint, very compact object similar to the sub-galactic, Lyα emission clumps found in other fields (Giavalisco et al. 1996; Pascarelle et al. 1996). Galaxy 1 is not detected in the deep STIS image and, although our measured Lyα flux is not inconsistent with this non-detection (see Sect. 3), this casts some doubt on the reality of this Lyα emitter whose flux is close to our 3σ detection limit.

No less than 20 Lyα absorptions are observed in the high-resolution spectrum of Outram et al. (1998) in the region corresponding to the bandpass of the NB filter. Their identification with any of the Lyα emitters is not straightforward. In particular, the associated metal system at $z_{\rm a}$=2.198 shows evidence for an incomplete coverage of the source, and is thus due to material located within the quasar inner structure. Spectroscopic confirmation of our Lyα emission candidates is needed to ascertain their association with Lyα absorbers.

There is no clear galaxy candidate associated with the weak Mg II doublet at $z_{\rm a}$=0.4143 detected by Outram et al. (1998). Either the galaxy is heavily blended with the quasar image or, alternatively, the associated galaxy could be at a larger radial distance ($> 10''$) than found for absorption-selected galaxies at similar redshifts associated with stronger Mg II systems (Bergeron & Boissé 1991). The impact parameter and luminosity of the $z_{\rm g}$=0.57 (Tresse et al. 1998), L* galaxy located 4.9″ north-east of the quasar are similar to those found for Mg II absorption-selected galaxies. We noted that the unidentified absorption line at 4390.66 Å (Outram et al. 1998) corresponds to Mg IIλ2796 at $z_{\rm a}$=0.5701. This line, together with another one at 4401.89Å, is also present in a spectrum obtained at the NTT with the EMMI spectrograph (V. d'Odorico et al., private communication) which confirms the existence of a Mg II absorption doublet associated with the $z_{\rm g}$=0.57 galaxy.

Acknowledgements. We are deeply grateful to members of the Science Verification Calibration team, B. Leibundgut and G. de Marchi, for their invaluable work. We are also greatly indebted to S. d'Odorico for his initiative in providing the narrow-band filter. This work was partially supported by the network "Formation and Evolution of Galaxies" set up by the European Commission under contract ERB FMRX-CT96-086 of its TMR programme.

References

Baugh C.M., Cole S., Frenk C.S., Lacey C.G., 1998, ApJ 498, 504
Bergeron J., Boissé P., 1991, A&A 243, 344
Bertin E., Arnouts S., 1996, A&AS 117, 393
Bremer M.N., Fabian A.C., Sargent W.L.W., et al., 1992, MNRAS 258, 23P
Carswell R.F., Mountain C.M., Robertson D.J., et al., 1991, ApJ 381, L5
Espey B.R., Carswell R.F., Bailey J.A., Smith M.G., Ward M.J., 1989, ApJ 342, 666
Giavalisco M., Steidel C.C., Macchetto F.D., 1996, ApJ, 470, 189
Heckman T.M., Lehnert M.D., Miley G.K., van Breugel W., 1991, ApJ 381, 373
Heckman T.M., Lehnert M.D., van Breugel W., Miley G.K., 1991, ApJ 370, 78
Hopkins A., 1998, http://www.atnf.csiro.au/~ahopkins/hdfs/source.html
Hu E.M., McMahon R.G., 1996, Nature 382, 231
Hu E.M., Songaila A., Cowie L.L., Stockton A., 1991, ApJ 368, 28
Hu E.M., Cowie L.L., McMahon R.G., 1998, ApJ 502, L99
Lowenthal J.D., Koo D.C., Guzman R., et al. 1997, ApJ 481,673
Madau P., Ferguson H.C., Dickinson M.E., et al., 1996, MNRAS 283, 1388
Madau P., Pozzetti L., Dickinson M., 1998, ApJ 498, 106
McCarthy P.J., Spinrad H., van Breugel W., 1995, ApJS 99, 27
McCarthy P.J., Baum S.A., Spinrad H., 1996, ApJS 106, 281
Mo H.J., Mao S., White S.D.M., 1998, MNRAS 295, 319
Omont A., Petitjean P., Guilloteau S., et al., 1996, Nature 382, 428
Outram P.J., Boyle B.J., Carswell R.F., et al., 1998, MNRAS, in press, astro-ph/9809404
Pascarelle S.M., Windhorst R.A., Keel W.C., Odewahn S.C., 1996, Nature 383, 45
Petitjean P., Pécontal E., Valls-Gabaud D., Charlot S., 1996, Nature 380, 411
Savaglio S., 1998, AJ 116, 1055
Sealey K.M., Drinkwater M.J., Webb J.K., 1998, ApJ 499, L135
Steidel C.C., Giavalisco M., Pettini M., Dickinson M., Adelberger K.L., 1996a, ApJ 462, L17
Steidel C.C., Giavalisco M., Dickinson M., Adelberger K.L., 1996b, AJ 112, 352
Steidel C.C., Adelberger K.L., Giavalisco M., Dickinson M., Pettini M., 1998, ApJ, submitted, astro-ph/9811399
Tresse L., Dennefeld M., Petitjean P., Cristiani S., White S., 1998, A&A, submitted, astro-ph/9812246
van Ojik R., 1995, PhD Thesis, Sterrewacht Leiden, p. 29
van Ojik R., Röttgering H.J.A., Carilli C.L., et al., 1996, A&A 313, 25